Scientific Research Publishing

Open Journal of Physical Chemistry, 2021, 11, 106-127
https://www.scirp.org/journal/ojpc
ISSN Online: 2162-1977
ISSN Print: 2162-1969

Methylene Blue Dye Adsorption onto Polyoxometalate Ionic Liquid Supported on Bentonite: Kinetic, Equilibrium and Thermodynamic Studies

Norah Alsubaie, Rawan Alshamrani, Doaa Domyati, Nadiyah Alahmadi, Fatma Bannani

Department of Chemistry, College of Science, University of Jeddah, Jeddah, Saudi Arabia
Email: fmdriss@uj.edu.sa

How to cite this paper: Alsubaie, N., Alshamrani, R., Domyati, D., Alahmadi, N. and Bannani, F. (2021) Methylene Blue Dye Adsorption onto Polyoxometalate Ionic Liquid Supported on Bentonite: Kinetic, Equilibrium and Thermodynamic Studies. *Open Journal of Physical Chemistry*, **11**, 106-127.
https://doi.org/10.4236/ojpc.2021.112006

Received: April 23, 2021
Accepted: May 23, 2021
Published: May 26, 2021

Abstract

The potential of polyoxometalate ionic liquid POM-IL supported on low-cost and available eco-friendly Saudi raw bentonite in the adsorption of MB cationic dye was investigated. For this purpose, $TOA_x[\alpha\text{-}XW_{11}O_{39}]$@Bentonite (X = Si, P; TOA = TetraOctylAmmonium), namely SWB and PWB were prepared and characterized by IR, XRD, XRF, SEM, TEM and BET. Batch adsorption experiments showed that SWB and PWB have higher adsorption capacity than the raw bentonite with an enhancement of about 37% for SWB. The adsorption capacities of both SWB and PWB improved with increasing contact time and temperature and decreased with higher salt concentration in solution. The pH is shown to have insignificant effect on the adsorption of MB onto SWB and PWB. This result is quite meaningful in the adsorption process application since it makes pH complicated adjustment of the discharged contaminated water before treatment unnecessary. The Kinetic study expressed that the pseudo-second-order model described the adsorption process better than the pseudo first order. The experimental isotherm data were found to fit the Langmuir model compared to the Freundlich model with a maximum adsorption capacity 277.78 mg/g and 113.6 for PWB and SWB respectively. The thermodynamic parameters illustrated that the adsorption process was favorable, spontaneous and endothermic.

Keywords

Adsorption, Bentonite, Polyoxometalates, Ionic Liquid, Wastewater Treatment

1. Introduction

Water pollution became the most challenging environmental issues in many

countries, due to the industrial rapid development [1] [2]. Dyes as worst type of water pollutants [3] [4] are toxic and have an important ecological impact on ecosystem due to their strong hazard, bioaccumulation, and environmental persistence [5].

Discharge of dyes from various industrial sources such as textile, paper, food and cosmetics without treatment into the water bodies has a badly effect on ecosystem [6] [7].

Dyes can be divided into several categories, whether anionic or cationic dyes. Methylene Blue, as a typical cationic dye, was predominantly selected as a model compound to examine the adsorption process due to its wide range application in textile industries [4] [8].

A variety of conventional techniques consisting of physical, physicochemical and biological treatment have been used for the removal of dyes [9] [10] [11] [12].

Adsorption as, physicochemical treatment, is considered a technique of choice due to its low-cost, effectiveness, and easy adaptation [13].

Polyoxometalates POMs as transitional metal-oxygen clusters, are a class of inorganic compounds having tunable properties and versatile applications in different fields such as catalysis, materials science, medicine… [14] [15]. The Polyoxometalates clusters can be associated with massive organic cations to give versatile liquid materials (POM-IL) and offer several properties required for water decontamination [16] [17] [18]. On the other hand, POMs have low surface area; this disadvantage can be overcome by incorporation of the POM in different stable porous supports by formation of various composites.

Several groups have reported some adsorbents for water purification from dyes which include activated carbon, fly ash, zeolite, red mud and polymers. These adsorbents have many drawbacks such as high cost and difficult regeneration and long time to achieve adsorption equilibrium, thus limiting the application use of adsorption method in dye removal in large scale. Bentonite can be used as potential support, because it has the advantages to be naturally abundant, inexpensive, eco-friendly, having good surface area and good cation exchange capacity [19] [20].

This work aims to assess the potential for using a new adsorbent based on supported POM-IL on bentonite in the removal of MB dye from aqueous solutions. The adsorption characteristics will be investigated under operating variables, such as contact time, adsorbent mass, initial MB concentration, pH solution and temperature. Isotherm, kinetics and thermodynamic studies were performed in order to evaluate the adsorption process that controlled the removal of MB from aqueous solutions.

2. Materials and Methods

2.1. Materials

Bentonite was collected from Khulays bentonite deposit, 95 km north of Jeddah,

Saudi Arabia. All reagents used were analytical grade and were not subjected to additional purification. Analytical grade Methylene Blue (MB) ($C_{16}H_{18}ClN_3S$), supplied from Fluka was used without further purification. Sodium tungstate Na_2WO_4, salts, namely sodium chloride (NaCl), potassium chloride (KCl) and sodium nitrate ($NaNO_3$) were all obtained from J.T. Baker. Distilled water was used to prepare all aqueous solutions in the study.

2.2. Adsorbent Preparation

The adsorbent preparation was preformed according to three steps.

First monolacunary Keggin-type polyoxometalates preparation, then preparation of polyoxometalate Ionic liquid POM-IL by metathesis reaction, followed by impregnation of the raw clay.

2.2.1. Synthesis of K_8 [α-$SiW_{11}O_{39}$]·$13H_2O$

The polyanion was prepared according to the reported literature procedure [18]. $Na_2WO_4{\cdot}4H_2O$ (182 g, 0.55 mol) is dissolved in distilled water (300 mL) and the solution is heated to reflux. Aqueous 4M HCl (165 mL) is added dropwise under vigorous stirring to the heated solution over a period of 30 min. Crucially, any precipitate (tungstic acid) formed is allowed to re-dissolve before further acid addition. An aqueous solution of sodium metasilicate (11 g, 50 mmol in 100 mL distilled water) is added followed by quick addition of aqueous 4M HCl (50 mL), giving a solution pH of 5.0. The solution is refluxed for 1 h.

After cooling to room temperature, KCl (150 g) is added, and a colorless precipitate is formed. The solid product is collected by filtration, washed with two 50 mL portions of aqueous KCl solution (1 M) followed by two 30 mL portions of cold water. The crude product is recrystallized from water, filtered and the colorless crystalline product is dried in the desiccator under vacuum.

2.2.2. Synthesis of K_7 [α-$PW_{11}O_{39}$]·$13H_2O$

The undecatungstophosphate was prepared using the same method according to the literature procedure. [18]

In 300 mL beaker, 54 g of $Na_2WO_4{\cdot}2H_2O$ (0.164 mole) and 2.1 g of Na_2HPO_4 (0.015 mole) were dissolved in 150 mL distilled water. The solution was heated and stirred at 90˚C and 60 mL of (4 M) HCl was added dropwise by burette over one hour. The final pH of the solution should be adjusted to 5.5 - 6.5, if necessary. The solution was kept at 90˚C for another hour and the pH was checked again. If the pH remained unchanged, 21 g of solid KCl was added to the solution and dissolved. Upon cooling to 0˚C the white precipitate was isolated from the solution, and it was recrystallized twice from hot water. The salt was checked with IR and EDS and the results were in agreement with those reported in literature.

2.2.3. Synthesis of TOA_x [α-$XW_{11}O_{39}$] (X = Si, P)

In a round-bottom flask, a solution of K_y [α-$XW_{11}O_{39}$]·xH_2O (1.00 eq.) was dissolved in 50 mL of water, heated to 50˚C and a solution of adequate amount of TOA-Br (8.00 eq for $\{SiW_{11}O_{39}\}$ and 7.00 for $\{PW_{11}O_{39}\}$) in toluene (80 mL) was

added. The mixture was vigorously stirred for 5 minutes and the organic layer was separated. After removal of the solvent under reduced pressure, the light yellow highly viscous liquid was solvent-stripped once with 50 mL toluene and three times with 50 mL chloroform.

2.2.4. Synthesis of TOA_8 [α-$XW_{11}O_{39}$]@Bentonite (X = Si Namely SWB, X = P Namely PWB)

0.5 g of $[N(C_8H_{17})_4]_yXW_{11}O_{39}$ was dissolved in 50 mL of acetone and then 4 g of Bentonite were added. The suspension was gently shaken for 30 minutes and the solvent was removed by rotary evaporator. Further 50 mL of acetone were added, and the shaking/solvent removal procedure was repeated three times. The final product was obtained as a solid, free-flowing powder. The POM-IL loading corresponds to 12.5 wt%.

2.3. Characterizations of SWB and PWB

Information on the crystalline structures was obtained through XRD analysis (powder PXRD diffractometer (Model Equinox 1000-INEL (France) with Co K_α (λ = 1.7890 Å) radiation at 30kV and 30mA. Comparison of POMs to the parent Keggin structure was performed using the reference data in the ICDD (international Centre for Diffraction Data) database. Sample morphology was investigated by means of field emission scanning electron microscopy (FEG-SEM, Quanta FEG450. FEI, the Netherlands) using an ETD Everhart Thornley detector (High Vacuum mode), a solid-state backscattering electron detector (VCD) and EDS detector (XFLASH6-30, Brucker) for the determination of elemental composition of the samples. The dispersion as well as size of POMs particles on the Bentonite support and the layered structure of Bentonite and POM-IL@Bentonite were confirmed by transmission electron microscope (TEM) using a Tecnai G2 F20 Super Twin (FEI, the Netherlands) with a LaB6 source at 200 kV. The electron microscope was fitted with an EDS detector used for elemental analysis. The nanoprobe STEM imaging were performed with a HADAF detector. Gatan camera 200 kV, 2kx2k resolution was used to collect TEM images. The TEM, HRTEM, STEM and EDS data were collected and treated by using the TIA software (Tecnai Imaging and Analysis software version 1.9.162) and Gatan Micrograph Software version 2.3.

POM-IL and bentonite surface functional groups were investigated using Fourier transform infrared spectroscopy (FTIR) analysis (Bruker Tensor II spectrometer).

Nitrogen sorption was used to investigate the specific surface area (BET method), specific pore volume and pore diameter (BJH method) of the raw bentonite and POM-SIL modified bentonite using NOVA (2200 e) high-speed surface area and pore size analyzer.

2.4. Preparation of Adsorbate

Stock solution of 1000 mg/L was prepared by dissolving a 1 g of Methylene Blue

in 1 L of distilled water. The experimental solution was prepared by using distilled water for diluting the stock solution. The concentration of Methylene Blue dye before and after adsorption were determined using UV spectrophotometer, GENESYS 10S UV-VIS. The λ_{max} of MB dye has been estimated at 665 nm as shown in Figure 1.

2.5. Adsorption Experiment

2.5.1. Batch Method

Adsorption test for MB removal from aqueous solutions was examined using adsorption batch experiments to explore the adsorption properties and the factors influencing the adsorption. Batch experiments were performed by varying contact time, mass of adsorbents, concentration of dyes, pH, ionic strength and temperature.

The following conditions were preserved for the different sets of experiments:

1) The effect of pH was conducted in the range from 2.0 to 10.0, 30 mg of SWB and 40 mg of PWB, 100 mL solution volume, 50 ppm MB concentration and T = 298 K. HCl(0.01 M) or NaOH (0.01 M) was added to set the desired pH value.

2) Effect of contact time was carried out through the time intervals (10, 20, 30, 40, 50, and 60 min), 30 mg of adsorbent, 100 mL solution, 50 ppm MB concentration, 298 K, initial non modified pH.

3) The effect of adsorbent mass was examined using different doses (20, 30, 40 and 50 mg) of adsorbent, initial non modified pH, time 60 min, 50 ppm MB concentration, 100 mL solution volume, and temperature 298 K.

4) The effect of initial concentration was conducted using 50, 100, 150 and 200 mg/L of MB, initial non modified pH, time 60 min, adsorbent mass 30 mg of SWB and 40 mg of PWB, and temperature 298 K.

5) The Effect of ionic strength was conducted by adding NaCl, KCl and $NaNO_3$ salts at different concentrations ranging from 0.1 to 0.4 M, initial non modified pH, time 60 min, 50 ppm MB concentration, 100 mL solution volume, and temperature 298 K.

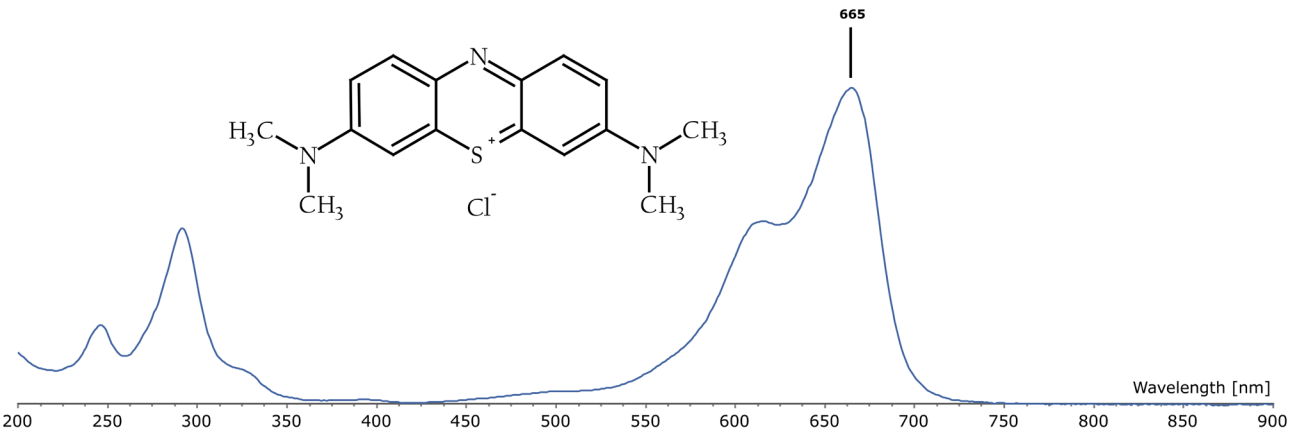

Figure 1. Absorbance of methylene blue (MB) at λ_{max} = 665 nm (C = 5 mg/L).

6) The influence of temperature on the adsorption process was studied under different temperatures of 298, 313, 328 and 343 K, initial non modified pH, time 60 min, 50 mg/L MB concentration, adsorbent mass 20 mg, solution volume 100 mL.

In all experiments, a water bath shaker at 300 rpm was used to set the desired temperature and duration of the studied mixture. After adsorption, the dye was kept apart from the adsorbent by centrifugation with 3000 rpm speed and use UV-VIS spectrophotometric technique to determine the residual concentration C based on Beer-lambert equation.

2.5.2. Data Processing

The percentage removal and adsorption capacity at time (Q_t) were calculated by using Equations (1) and (2), respectively.

$$R\% = \frac{C_0 - C_f}{C_0} \times 100 \quad (1)$$

$$Q_t = \frac{C_0 - C_f}{m} \times V \quad (2)$$

C_0 and C_t: initial and final concentrations (mg/L) of dye solutions. V: volume (L). m: mass (g) of the adsorbent.

2.6. Reusability Test

The reusability of the adsorbent was examined for four adsorption cycles. Adsorption was performed in 50 mg/L Methylene Blue (MB) solution with 400 mg absorbent at room temperature, after removing MB dye, the MB-loaded adsorbent was washed with 80 mL of 5% HCl/ethanol (v/v) and washed twice with distilled water for 15 minutes and then dried at 120˚C for reuse in a fresh contaminated solution.

3. Results and Discussion

3.1. Characterization of SWB and PWB

3.1.1. Fourier Transform Infrared (FTIR)

The FTIR spectra of raw bentonite, SWB and PWB in the range of 4000 - 400 cm^{-1} were shown in **Figure 2**. The FTIR transmittance bands in the low frequency region (1200 - 400 cm^{-1}) of the modified Bentonite and raw Bentonite are largely comparable indicating that the clay mineral has not changed upon modification by polyoxometalate.

Absorption due to Al-O-Si bending at 527 cm^{-1}, Si-O-Si bending at 468 cm^{-1}, and Al-Al-OH bending at 914 cm^{-1} confirm the presence of montmorillonite [21] [22]. The very strong characteristic peak observed at 1032 cm^{-1} was ascribed to asymmetric stretching vibrations of Si-O-Si bonds. The broad band in the 3430 - 3623 cm^{-1} region can be ascribed to the symmetric stretching of (Si-OH, Al-OH) structural hydroxyl groups OH and of the physically adsorbed water OH. The shoulder at 3694 cm^{-1} and the weak band at 695 cm^{-1} suggest the presence of kaolinite. The absorption band at 1639 cm^{-1} is attributed to the

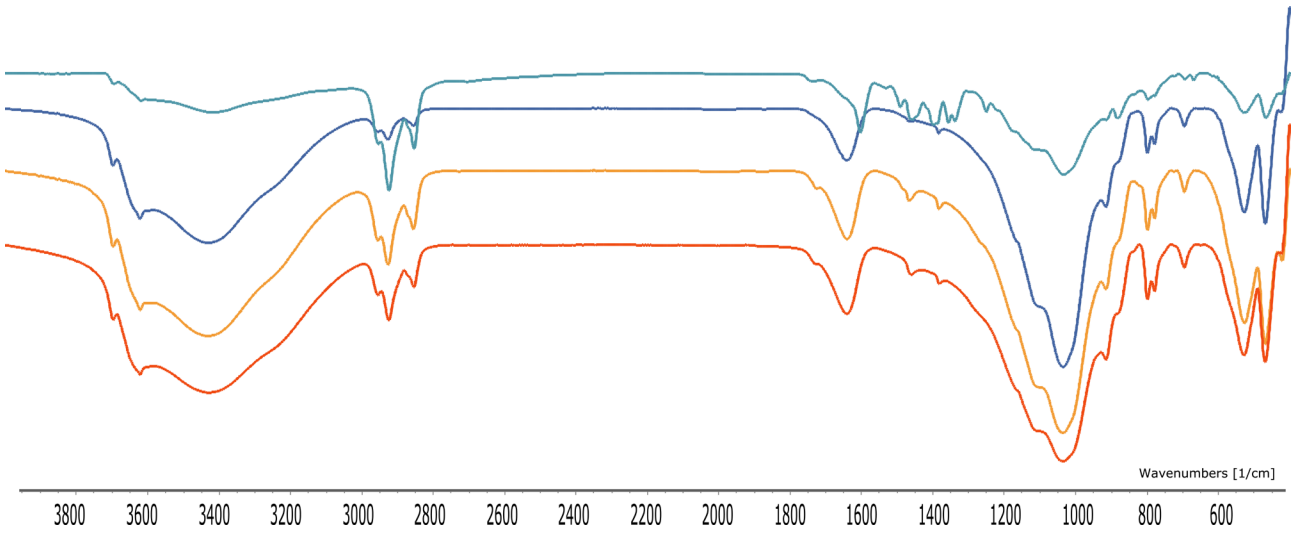

Figure 2. Infrared spectra (from top to bottom) of SWB after MB adsorption, SWB before adsorption, PWB and Bentonite.

angular vibration of the OH group and related to the adsorbed water and the hydration water present in the clay.

New absorption bands emerged at 2950, 2854, 1468 and 1382 cm^{-1} which confirm the presence of TOA cations. The fingerprint of POM is not clearly visible in FT-IR spectra of SWB and PWB due to their overlapping with FT-IR bands of Bentonite.

After adsorption of MB dye some bands appeared, such as bands at 1488 cm^{-1} and peaks at 1394 - 1335 cm^{-1} region related to the $-CH_3$ and the feature conforming to the C=C skeleton stretching at 1600 cm^{-1} characteristic of the aromatic ring vibrations of MB dye.

3.1.2. Scanning Electron Microscope Analysis (SEM)

The SEM images of the raw Bentonite showed an irregular porosity and disperse surface with large number of cavities **Figure 3(A)**. In contrast, the morphology of SWB sample showed clear changing in the surficial properties of the clay **Figure 3(B)**. The surface becomes smoother, flake like morphology with smaller cavities than raw bentonite, this result is confirmed by BET analysis. The Scanning Electron Microscopy showed that the bentonite layer-stacking structure was retained even after incorporating polyoxometalate ionic liquid into the bentonite matrix.

3.1.3. Chemical Composition

EDS analysis **Table 1** showed that natural Saudi bentonite is mainly composed of silicon dioxide, Aluminum oxide, iron oxide, sodium oxide, in addition to calcium, magnesium, titanium and potassium oxides. Comparison of raw and modified bentonite revealed no significant change of the chemical composition of the bentonite matrix.

3.1.4. Powder X-Ray Diffraction (PXRD)

The X-ray patterns of raw Bentonite, PWB and SWB are illustrated in **Figure 4**.

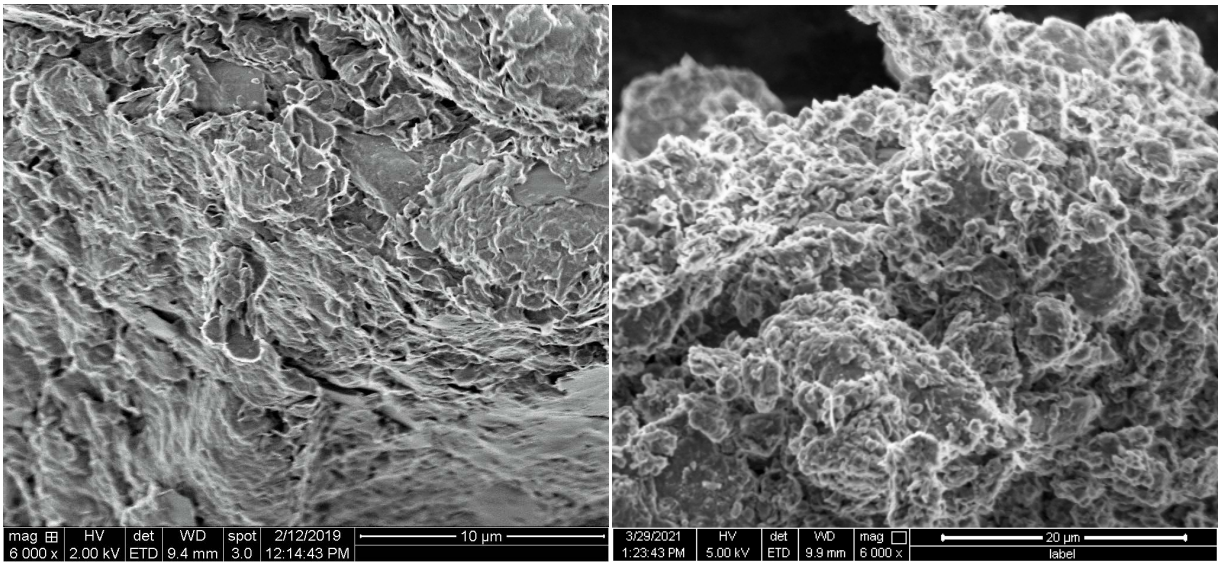

(A) (B)

Figure 3. SEM images of (A) natural bentonite and (B) SWB.

Table 1. Chemical composition of raw Saudi bentonite and POM-IL modified bentonite.

Main constituent	SiO_2	Al_2O_3	Fe_2O_3	MgO	TiO_2	Na_2O	CaO	K_2O
Raw Bentonite Wt%	59.03	21.59	9.63	2.95	1.37	2.83	1.24	0.66
Modified Bentonite Wt%	58.11	19.58	10.06	2.15	1.69	1.43	1.39	0.63

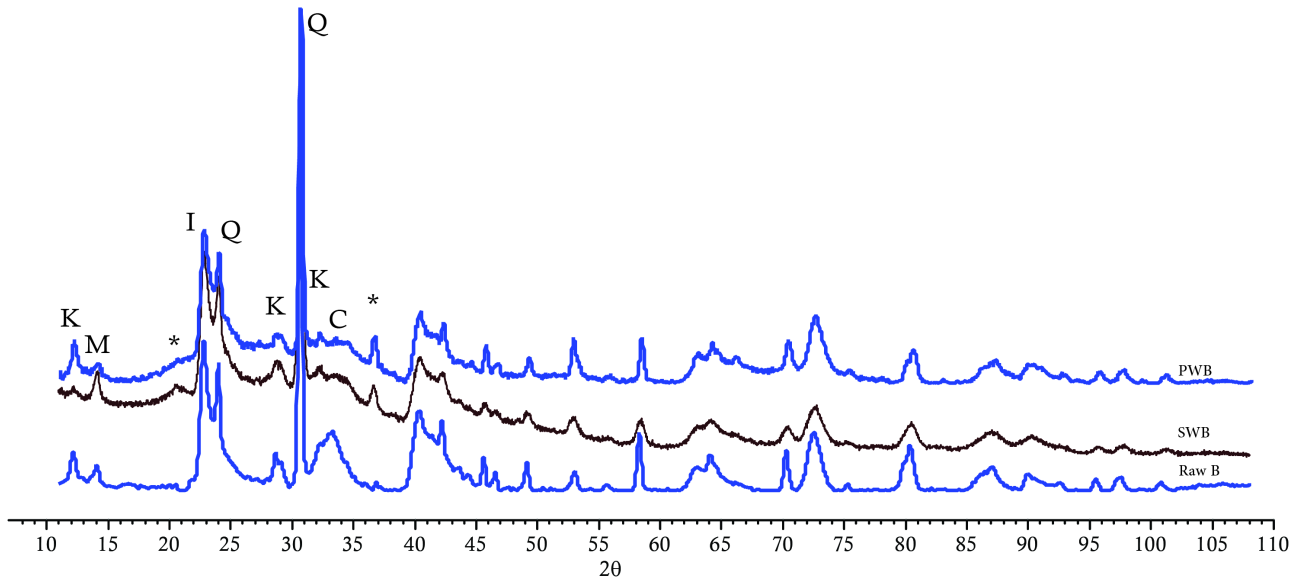

Figure 4. XRD analysis of (from top to bottom) SWB, PWB and raw bentonite (* = pom peaks).

The XRD analysis of raw bentonite sample showed that bentonite is mainly composed of, quartz (SiO_2), calcite ($CaCO_3$) and Feldspar as non-clay minerals.

XRD patterns diffractograms revealed three main clay minerals, montmorillonite, kaolinite and illite. Moreover, the characteristic diffraction signals were found to be identical for both raw bentonite and $(TOA)_yXW_{11}$@Bentonite which

indicate that the POM-IL remains on the surface of the clay.

The X-ray diffractogram recorded in a range of small angle (2θ) ranging from 0˚ to 10˚ Figure 5 shows the presence of a characteristic diffraction peak located at (2θ) = 5.68˚ from which the interlayer distance was found to be 14.08 Å. This peak is associated with the (001) diffraction (d_{001}) of the montmorillonite phase. [23] [24] The introduction of POM to the Bentonite has not affected the d_{001} diffraction peak which appears at 14.86 Å for SWB and 15.58 Å for PWB since there is no significant expansion of interlayer space Δd (4.38Å and 5.05 Å).

This finding confirmed that the structure of Bentonite is retained after POM-IL incorporation.

Moreover, the presence of POM in the prepared adsorbent is confirmed by the presence of structural characteristic peaks at 2θ: 37.20˚, 65.80˚, 66.83˚ and 78.77˚ in agreement with the Keggin structure [25] [26]. The data also show that quartz major component is not affected during POM incorporation to the clay.

3.1.5. Transmission Electron Microscopy Analysis (TEM)

TEM characterization carried out on the raw bentonite and POM modified bentonite are presented in Figure 6(A). TEM analysis confirmed the XRD results and reveal the existence of layers at basal space d_{001} = 14.08Å for bentonite and d_{001} = 14.75 Å for POM modified bentonite. Moreover, TEM shows that POM molecules are located on the surface of Bentonite (dark spots in Figure 6(B)) and confirm the nanosized Keggin structure (~1 nm).

3.1.6. Nitrogen Sorption Analysis

Nitrogen sorption was used to investigate the specific surface area (BET method), pore diameter and specific pore volume (BJH method) of the raw bentonite and

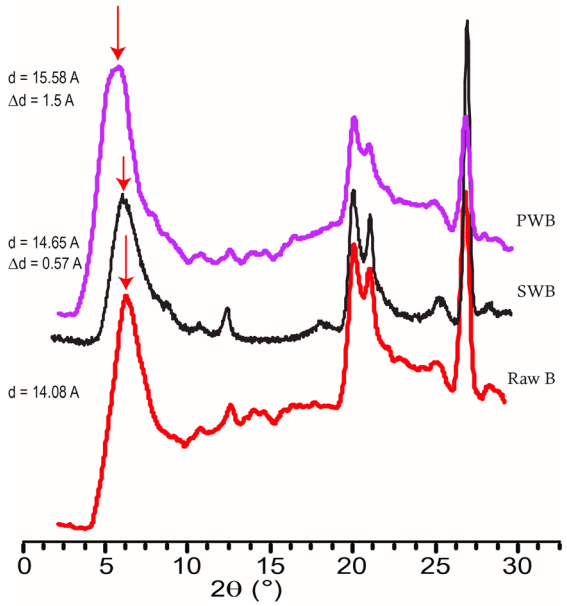

Figure 5. Low angle PXRD diffractograms of (from top to bottom) SWB, PWB and raw bentonite.

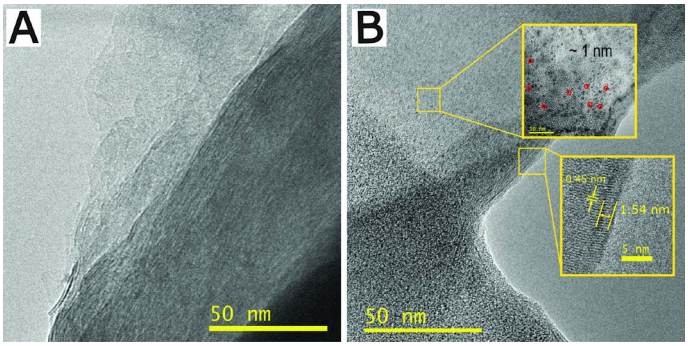

Figure 6. TEM images of: (A) Raw bentonite and (B) SWB.

Table 2. Nitrogen sorption results for non-modified bentonite and POM-IL modified bentonite.

Samples	Specific surface area (m^2/g)	Specific pore volume (cm^3/g)	Average pore radius (Å)
Raw Bentonite	59	0.086	17.60
PWB	1.16	0.013	14.83
SWB	2.32	0.015	15.58

POM-IL modified bentonite to establish the consequences of POM-IL adsorption on the bentonite pore structure. The data in Table 2 show that upon POM-IL adsorption in POM-IL@bentonite, an overall reduction in pore diameter, specific pore volume and specific surface area is observed. This verifies that the POM-IL does not only coat the exterior surface but also coats the internal pore structure while leaving the pores still accessible.

3.2. MB Adsorption Experiments

3.2.1. Effect of Contact Time

The effect of contact time on Methylene Blue removal by SWB, PWB and bentonite is shown in Figure 7. It could be seen that the MB adsorption increases with increasing contact time for modified and raw bentonite and occurred in two stage: first fast stage and equilibrium stage. SWB adsorbent has higher removal than PWB during the rapid first stage and reached 93% removal after 10 min compared to 66% for PWB for the same time. The difference can be explained by the nature of the heteroatom in the polyoxometalate which plays a role in the overall charge of the polyanion making $[SiW_{11}O_{39}]^{8-}$ more negative than $[PW_{11}O_{39}]^{7-}$ which in turn attracts more cationic MB dye since the adsorption is due to electrostatic attraction between negative adsorbent surface and positive dye molecules. The rapid MB removal during the first stage (10 min) is due to presence of high number of available vacant sites on the adsorbent surfaces, the adsorption reached equilibrium within almost 30 min with total removal. Further increase in contact time will no longer improve the adsorption percent removal. There is also a significant difference in percent removal between raw bentonite, SWB and PWB which clearly confirms the enhancement in

bentonite adsorptive performance with POM-IL modification.

3.2.2. Effect of Adsorbent Mass

The effect of adsorbent mass was studied by variation of SWB and PWB dose from 20 to 60 mg. Figure 8(A) clearly shows that the % removal of MB increased with increasing dose of adsorbents. This is due to the increasing available vacant sites which, therefore increases the percent removal. However, the adsorption capacity (Q_e) Figure 8(B) decreased as the adsorbent dose increased. This is because, the large adsorbent mass effectively decreases the number of covered sites per unit mass comes down, which results in a reduced capacity.

By comparison with raw bentonite, we noticed that the capacity uptake of POM-IL bentonite for both adsorbents SWB and PWB is higher than that of raw bentonite in the range of 20 - 60 mg. such a result shows clearly that the incorporation of POM-IL in the bentonite matrix enhances the adsorptive capacity of the bentonite at low adsorbent dose.

3.2.3. Effect of Concentration

The effect of initial concentration on the removal of methylene blue on SWB,

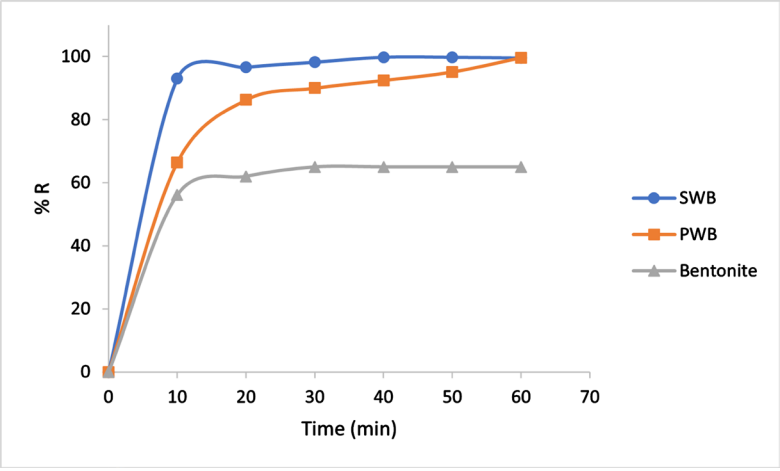

Figure 7. Effect of contact time on the adsorption of MB using SWB, PWB and bentonite.

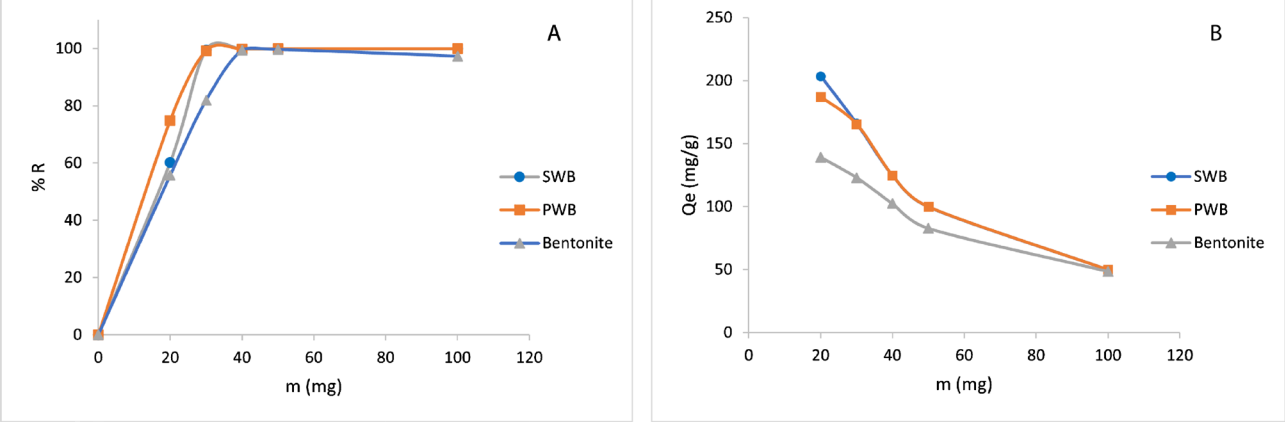

Figure 8. Effect of adsorbent mass of MB on SWB, PWB and Bentonite on the (A) % removal, (B) adsorption capacity Q_e.

PWB and bentonite is studied in the range from 50 - 200 mg/L. The results are reported in Figure 9. Several studies have documented the effect of initial dye concentration on dye uptake by clays. In most cases the increase of initial concentration resulted in an increase of the adsorption capacity and a decrease of the overall removal efficiency. In this study, the % removal of dye decreased with increasing initial dye concentrations. At low concentration (50 ppm), the removal reached almost 100% for both POM-IL modified bentonite and raw bentonite. Over loading of methylene blue above the saturation level did not find available vacant site resulting on the formation of accumulation of methylene blue molecule on the surface of adsorbent and the % removal decrease. At concentrations higher than 100 ppm, SWB adsorbent has higher % removal when compared to PWB and Bentonite which have similar results. The adsorption capacity (Q_e) increased gradually with the increase in concentration Figure 9(A). However, at lower dye concentration, the adsorption is independent on initial concentration since the ratio of the number of MB cations to the number of available adsorption sites is small.

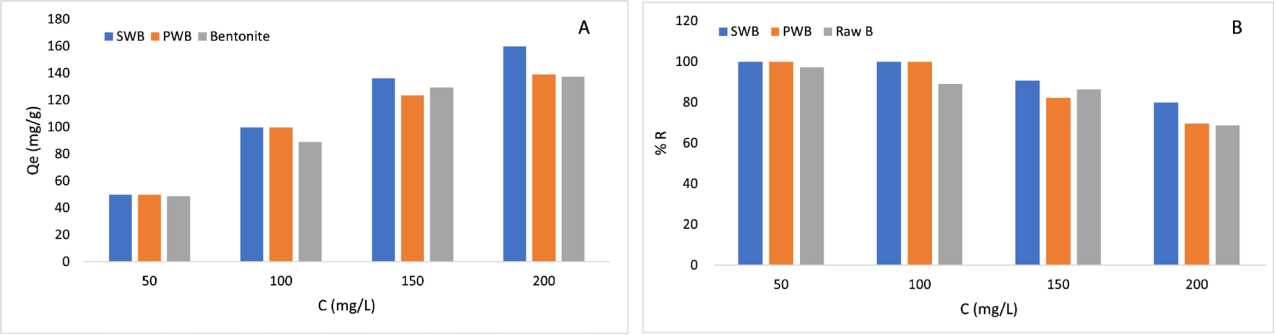

Figure 9. Effect of initial concentration Effect of initial concentration on the % removal (A) and adsorption capacity (B).

3.2.4. Effect of pH

The pH effect on the adsorption of MB dye on SWB and PWB was investigated in the range of 2 - 10. As shown in Figure 10, there is no significant effect on the adsorption of methylene blue while changing the pH solution values, SWB and PWB are stable adsorbents over a wide pH range. Independent of the origin of this insignificant effect of the pH, this finding is quite meaningful in the adsorption process application since it makes complicated pH adjustment of the effluent before treatment unnecessary.

As a result, pH was not adjusted during adsorption experiments to simulate real treatment condition of industrial effluents.

3.2.5. Effect of Temperature

The effect of temperature on MB dye adsorption onto SWB and PWB was conducted at 5 different temperatures ranging from 303 to 343 K.

Figure 11 shows that the removal percentage of MB increased with the increase in temperature, indicating that MB adsorption on both adsorbent surfaces was favored at higher temperatures. The increase in adsorption with increasing

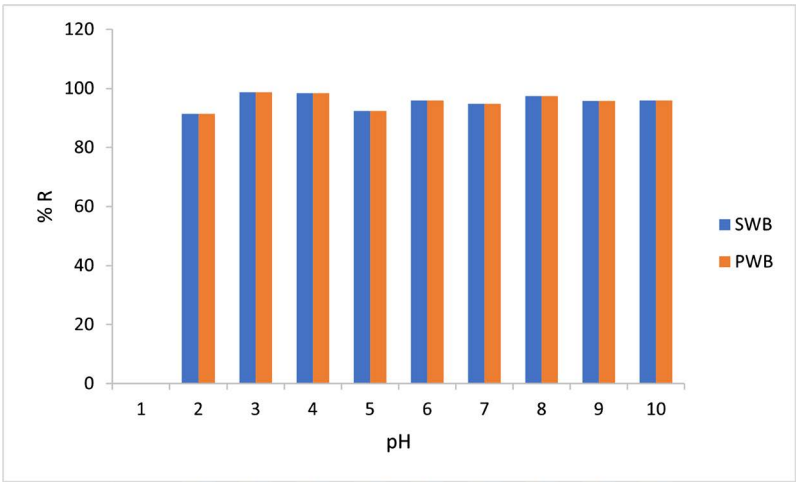

Figure 10. Effect of pH on the adsorption of MB by SWB and PWB.

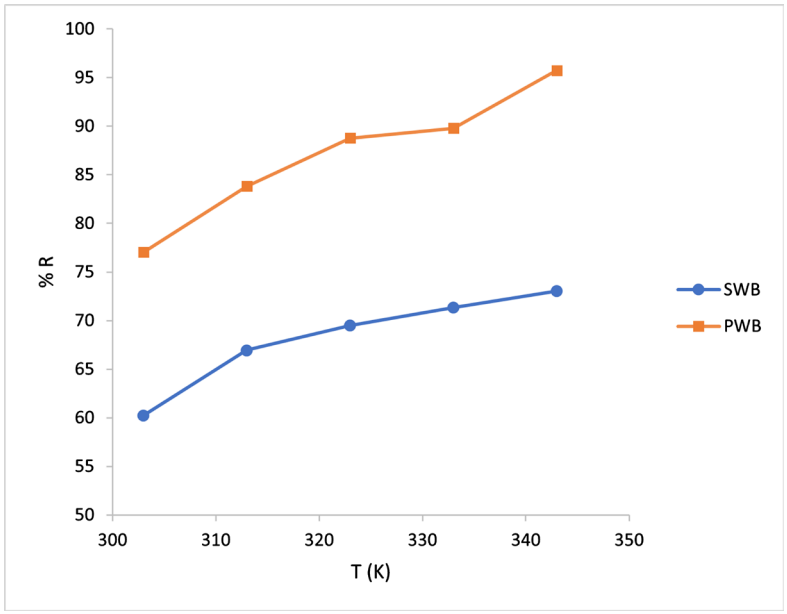

Figure 11. Effect of temperature on the adsorption of MB by $TOAPV_3W_9$@clay.

temperature indicated the endothermic nature of the adsorption process.

3.2.6. Effect of Ionic Strength

The study the effect of salts on the adsorption of dyes is important since wastewater contains different concentrations of salts **Figure 12** shows the influence of salt concentration on MB adsorption onto SWB and PWB. As a whole, the presence of salts reduced the capacities of SWB and PWB on adsorbing MB dye. Both the % removal and the adsorption capacity of the POM-IL modified bentonite began to decrease when high concentrations of salts were added. This could be partly ascribed to the competitive adsorption between Na^+, K^+ and MB cations for available active sites. As shown in **Figure 12**, the reduced affinity between negatively charged POM-IL modified bentonite and MB cationic dye observed in presence of KCl is due K^+ smaller hydrated radius (2.32 Å) than Na^+

(2.76 Å); in this case K^+ could easily occupy more adsorption sites and could not as easily be leached. Similar results were reported by De Castro *et al.* when studying the adsorption of MB onto EDTA modified bentonite [27].

It is noticed that KCl inhibiting effect on the adsorption of MB is more pronounced in the case of SWB compared to PWB (Figure 12 and Figure 13).

The effect of chloride and nitrate anions on the MB adsorption is comparable Figure 13, because these negatively charged anions can compete with the bentonite as sites for electrostatic attraction and disrupt MB adsorption [27].

3.3. Kinetic Study

Adsorption kinetic describes the solute uptake rate and evidently this rate controls the residence time of adsorbate uptake at solid-solution interface. Two models were used to evaluate adsorption kinetics which are Pseudo-first order and Pseudo-second order kinetic models.

3.3.1. Pseudo First Order (Lagergren Model)

This model is one of the most extensively used models to describe the adsorption kinetics. The equation for pseudo-first order is:

$$\frac{\mathrm{d}t}{\mathrm{d}Q} = k_1 \left(Q_e - Q_t \right) \tag{3}$$

Q_t and Q_e are dye amount adsorbed (mg/g) at time, t (min) and at equilibrium, respectively, k_1 is the rate constant of adsorption (min^{-1}).

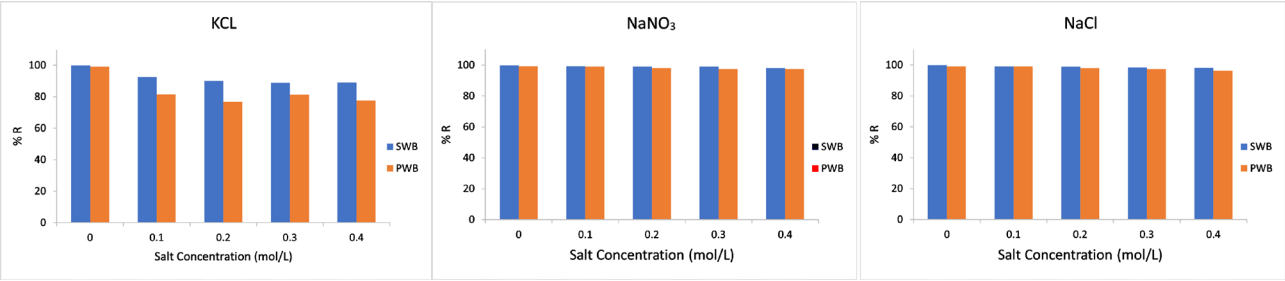

Figure 12. Effects of ionic strength on MB adsorption on SWB and PWB.

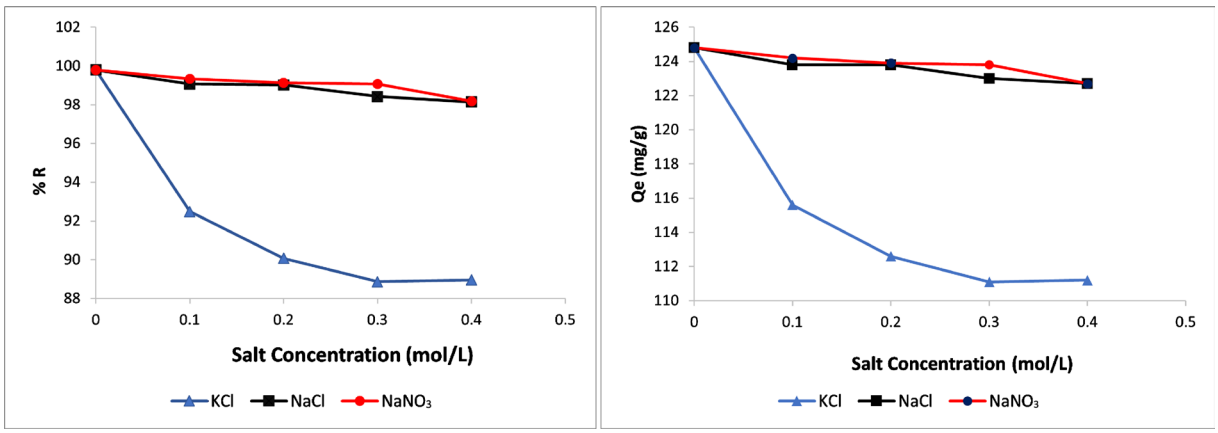

Figure 13. Effects of ionic strength on MB adsorption onto SWB.

The linear form for pseudo first order can be expressed as:

$$\ln\left(Q_e - Q_t\right) = \ln Q_e - k_1 t \tag{4}$$

When plot of $\ln\left(Q_e - Q_t\right)$ *vs* t drawn, Q_e and k_1 values can be obtained from intercept and slope respectively.

3.3.2. Pseudo-Second Order Model

Pseudo-second order suggests that the uptake process is due to chemisorption and has the general form as:

$$Q_t = \frac{k_2 Q_e^2}{1 + k_2 Q_e t} \tag{5}$$

Mathematically it can also be expressed as follows:

$$\frac{t}{Q_t} = \frac{t}{Q_e} + \frac{1}{k_2 Q_e^2} \tag{6}$$

where k_2 ((g/mg)/min) is the constant for second order, Q_e (mg/g) and Q_t (mg/g) the amount of dye adsorbed at equilibrium and any time respectively.

The kinetics of MB dye adsorption onto SWB and PWB were analyzed using pseudo-first-order PFO model (Equation (4)) and pseudo-second order PSO model (Equation (6)).

By applying the two kinetic model, it was found that the plot of t/q_t vs. t for PSO model fit for the whole range of contact time for both adsorbent, with excellent linearity Figure 14. On the other hand plots of $\ln\left(Q_e - Q_t\right)$ vs. t displayed less-linearity.

The kinetic parameters for PFO and PSO were calculated and tabulated in Table 3.

The real test for the validity of the kinetic model arises from the comparison between the experimentally determined q_e and the calculated q_e [28] [29]. According to the reported results it is clear that in the PSO kinetic model, the $Q_e cal$ is very close to the q_e *exp* values. In addition, the R^2 values > 0.99 for the PSO model were higher than those obtained in PFO model. Moreover, in pseudo-second-order a trend was observed with the rate constants, k_2 generally decreased as the initial concentration increases, which is due to the occupation of active sites. As a result of the above-mentioned reasons, it can be concluded that

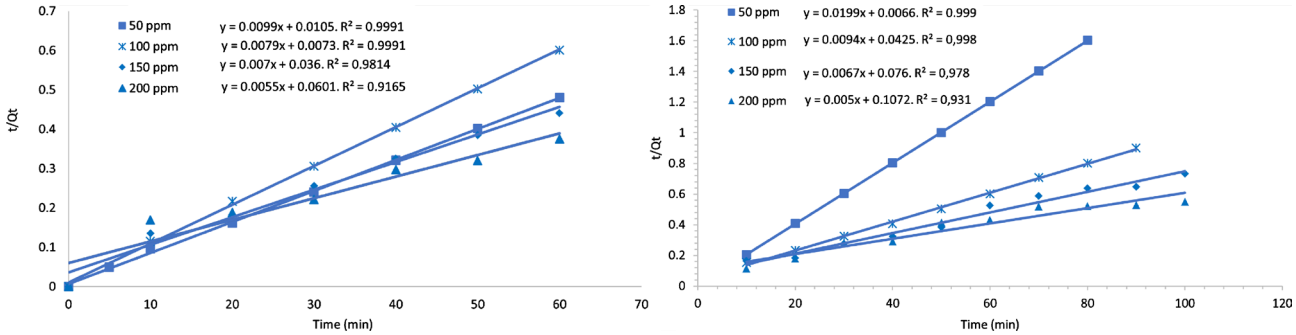

Figure 14. Pseudo-second-order kinetics plots for adsorption onto SWB (A) and PWB (B).

Table 3. Kinetic parameters for PFO and PSO models.

Adsorbent	C_0 (mg/L)	Q_eExp (mg/g)	Pseudo -first-order kinetic			pseudo-second-order kinetic		
			k_1 (min^{-1})	Q_eCal (mg/g)	R^2	k_2 (g/mg min)	Q_eCal (mg/g)	R^2
PWB	50	50	0.04	1.43	0.842	0.02	50	0.999
	100	99.9	0.0713	41.24	0.814	0.011	100	0.998
	150	140	0.0332	87.58	0.631	0.007	142	0.978
	200	182	0.048	349.67	0.515	0.005	200	0.931
SWB	50	50	1.040	2.83	0.365	0.02	50	0,999
	100	100	0.058	20.82	0.715	0.011	101	0.999
	150	147	0.063	209.9	0.813	0.001	154	0.987
	200	195	0.052	334.4	0.565	0.005	208	0.943

the pseudo-second-order model best fit the experimental equilibrium data.

3.4. Equilibrium Study: Adsorption Isotherm

Adsorption isotherms are mathematical models that characterize the distribution of the adsorbate types among liquid and adsorbent, based on a set of suppositions that are mainly related to the heterogeneity/homogeneity of adsorbents, the type of coverage and possibility of interaction between the adsorbate types.

They provide clear indication of the surface properties, affinity between the adsorbent and the adsorbate and the adsorption capacity of the adsorbent. Two equilibrium isotherm models were applied to interpret the experimental data for the adsorbent at different concentration to obtain the optimum values of the equilibrium parameters.

3.4.1. Langmuir Isotherm

The Langmuir isotherm assumes monolayer adsorption, absence of interaction between adsorbate molecules and homogeneous distribution of active sites on the adsorbent surface [22]. The general equation for Langmuir is:

$$Q_e = \frac{Q_{\max} k_L C_e}{1 + k_L C_e} \tag{7}$$

where, Q_e is the dye adsorbed amount at equilibrium (mg/g), $Q_{\max}$ is the maximum adsorption capacity (mg/g). k_L is the constant of Langmuir and C_e is dye concentration at equilibrium.

It can also be expressed as:

$$\frac{C_e}{Q_e} = \frac{1}{Q_{\max} k_L} + \frac{C_e}{Q_{\max}} \tag{8}$$

The value of $(1/Q_{\max})$ and K_L can be obtained from linear curve of (C_e/Q_e) versus C_e.

The R_L separation factor values provide information about the affinity between adsorbate and adsorbent which can be calculated using the following Eq-

uation (9):

$$R_L = \frac{1}{1 + k_L C_0} \tag{9}$$

where K_L is the Langmuir constant, C_0 (mg /L) is the initial concentration of dye.

Table 4 shows the types of Langmuir isotherm according to R_L Values.

3.4.2. Freundlich Isotherm

The Freundlich equation is empirical and assumes heterogeneous multilayer adsorption, its mathematical equation is express as:

$$Q_e = k_f C_e^{1/n} \tag{10}$$

where C_e is the equilibrium dye concentration (mg/L), Q_e is the dye adsorbed amount at equilibrium (mg/g), k_f are the Freundlich constants and n indicative of the extent of the adsorption and the degree of nonlinearity between solution concentration and adsorption intensity.

It can also be linearized in logarithmic form as shown below:

$$\log Q_e = \log k_f + \frac{1}{n} \log C_e \tag{11}$$

The value of $(1/n)$ and $\log k_f$ can be calculated from slope and the intercept respectively from linear plot of $\log Q_e$ verses $\log C_e$.

Table 5 summarizes the calculated coefficients of determination (R^2) and model parameters of the Langmuir and Freundlich isotherms. The results show clearly that the Langmuir isotherm ($R^2 > 0.98$ for SWB and $R^2 > 0.97$ for PWB) best fits the equilibrium data for both adsorbents. This indicates that MB adsorption onto SWB and PWB is homogeneous. The maximum adsorption capacities for MB onto SWB and PWB were 113 and 277 mg·g^{-1}, respectively.

To predict the adsorption efficiency, the essential characteristics of Langmuir isotherm was explained in term of a dimensionless constant separation factor R_L.

As shown in Figure 15(B), the R_L values calculated for both SWB and PWB

Table 4. Langmuir isotherm types according to R_L Values.

R_L	($R_L = 0$)	($0 < R_L < 1$)	($R_L = 1$)	($R_L > 1$)
Type of isotherm	irreversible	favorable	linear	unfavorable

Table 5. Adsorption Isotherm parameters of the MB on SWB and PWB.

Isotherm	Parameter	PWB	SWB
Langmuir	Q_{max} (mg/g)	277.78	113.6
	k_L (L/mg)	0.24	0.16
	R^2	0.972	0.985
Freundlich	n	13.08	5.122
	k_f (mg/g)	181.22	313.2
	R^2	0.879	0.860

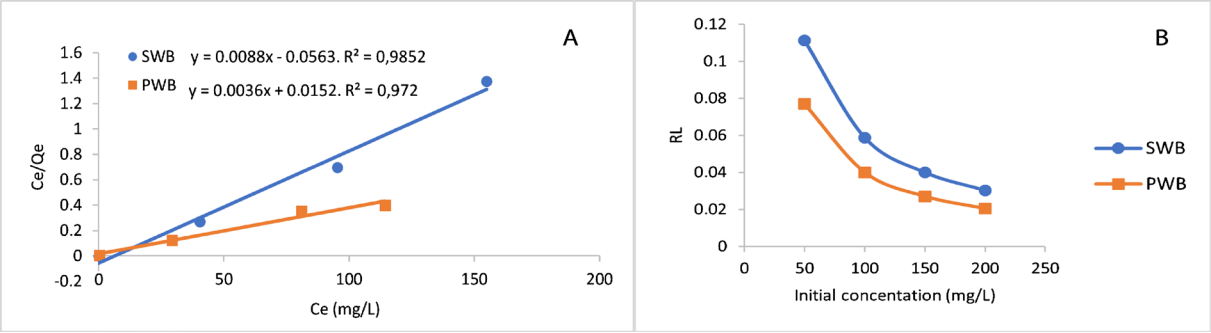

Figure 15. (A) Langmuir plot for adsorption of MB onto SWB and PWB. (B) Separation factor values (R_L) at varying initial MB onto SWB and PWB.

were all in the range of 0 - 1. Moreover, the R_L values were also observed to decrease when the MB dye initial concentration were increasing which means that the adsorption becomes more favorable. This could be due to the increase in driving force when more MB solute was present.

3.5. Thermodynamic Parameters

To evaluate the effect of temperature on the adsorption process, the standard Gibbs free energy $\Delta G°$, the standard enthalpy $\Delta H°$, were calculated using the below Equations:

$$\Delta G° = -RT \ln K_d \tag{12}$$

$$\ln K_d = \frac{-\Delta H°}{RT} + \frac{\Delta S°}{R} \tag{13}$$

$$K_d = \frac{Q_e}{C_e} \tag{14}$$

where K_d (Lg^{-1}) is the distribution coefficient, T(K): temperature expressed in Kevin and R is Gas constant (8.314 $J{\cdot}mol^{-1}{\cdot}K^{-1}$)

The standard entropy values (J/mol K), $\Delta S°$ were calculated using Gibbs-Helmholtz equation:

$$\Delta S° = \frac{\Delta H° - \Delta G°}{T} \tag{15}$$

The $\Delta G°$ values of MB adsorption onto SWB and PWB under different temperatures (303, 313, 323, 333 and 343 K) as well as $\Delta H°$ and $\Delta S°$ values are presented in Table 6.

MB dye adsorption process was spontaneous and endothermic which is proved by the negative value of $\Delta G°$ and positive value of $\Delta H°$. In addition, the $\Delta G°$ values became more negative at higher temperatures making the adsorption more favorable. Positive values of $\Delta S°$ indicate that the MB dye adsorption process increased the randomness during the adsorption process and suggest a strong affinity between MB and both adsorbents SWB and PWB.

3.6. Reusability Test

The ability of the adsorbents to be reused is a crucial factor. Reusability of the

Table 6. Thermodynamic parameters of the MB on SWB and PWB.

Adsorbent	T (K)	$\Delta G°$ (KJ/mol)	$\Delta H°$ (KJ/mol)	$\Delta S°$ ($J \cdot K^{-1} \cdot mol^{-1}$)
PWB	303	−0.272	35.014	116.62
	313	−1.429		
	323	−2.603		
	333	−2.986		
	343	−5.741		
SWB	303	−5.102	11.88	56.65
	313	−6.026		
	323	−6.530		
	333	−6.979		
	343	−7.426		

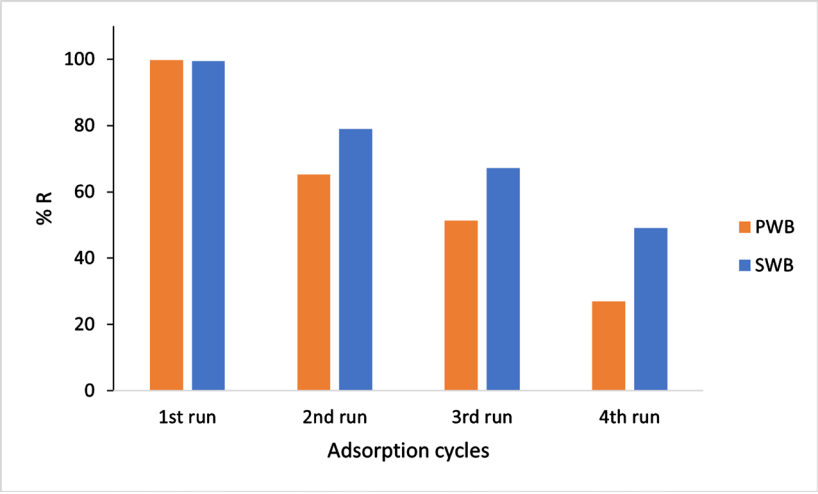

Figure 16. Reusability test for SWB and PWB adsorbent.

adsorbent is usually carried out in order to avoid the cost of a new acquisition and minimizing the amount of waste.

The recycled adsorbent indicated reasonable efficiency (100%) after one cycle and more than 50% after four and three runs for SWB and PWB respectively as shown in Figure 16. These results revealed that both SWB and PWB have a good potential as cost-effective adsorbent for removal.

4. Conclusions

In this study, new adsorbents based on polyoxometalate ionic liquid supported on Saudi bentonite were prepared and totally characterized. This surface modification was demonstrated to enhance the efficiency of Saudi raw bentonite in adsorbing MB cationic dye from aqueous solutions. In detail, the study was focused on the different parameters affecting the adsorption process, showing the role of the MB initial concentration, adsorbent dose, pH, temperature values and

ionic strength. The obtained data show that the adsorption process follows the PSO kinetic model. Adsorption isotherms are described by the Langmuir model confirming the homogeneous monolayer coverage of the adsorbent. The data obtained from the thermodynamic study at different temperatures were used to calculate the thermodynamic parameters and showed that the adsorption process onto POM-IL modified bentonite was found to be spontaneous, endothermic and favorable.

The possibility to perform consecutive cycles of adsorption using the same adsorbent was also presented. Overall, we can conclude that SWB and PWB can be used as an inexpensive, reusable, and environment-friendly treatment option for MB contaminated water. The POM-IL supported bentonite can have potential as multicomponent adsorbent in the removal of heavy metal due to the presence of lacunary polyoxometalate featuring metal binding sites (work in progress) and antibacterial activity owing to the presence of antimicrobial alkyl ammonium cations.

Conflicts of Interest

The authors declare no conflicts of interest regarding the publication of this paper.

References

[1] Bagheri, S., Muhd Julkapli, N. and Bee Abd Hamid, S. (2014) Titanium Dioxide as a Catalyst Support in Heterogeneous Catalysis. *The Scientific World Journal*, **2014**, Article ID: 727496. https://doi.org/10.1155/2014/727496

[2] Wan, K.T. and Davis, M.E. (1994) Design and Synthesis of a Heterogeneous Asymmetric Catalyst. *Nature*, **370**, 449-450. https://doi.org/10.1038/370449a0

[3] Rabbani, M., Seghatoleslami, Z.S. and Rahimi, R. (2017) Selective Adsorption of Organic Dye Methylene Blue by $Cs_4H_2PMo_{11}FeO_{40}\cdot 6H_2O$ in Presence of Methyl Orange and Rhodamine-B. *Journal of Molecular Structure*, **1146**, 113-118. https://doi.org/10.1016/j.molstruc.2017.05.134

[4] Sabarinathan, C., Karuppasamy, P., Vijayakumar, C. and Arumuganathan, T. (2019) Development of Methylene Blue Removal Methodology by Adsorption Using Molecular Polyoxometalate: Kinetics, Thermodynamics and Mechanistic Study. *Microchemical Journal*, **146**, 315-326. https://doi.org/10.1016/j.microc.2019.01.015

[5] Malachova, K., Rybkova, Z., Sezimova, H., Cerven, J. and Novotny, C. (2013) Biodegradation and Detoxification Potential of Rotating Biological Contactor (RBC) with *Irpex lacteus* for Remediation of Dye-Containing Wastewater. *Water Research*, **47**, 7143-7148. https://doi.org/10.1016/j.watres.2013.07.050

[6] An, S., Liu, X., Yang, L. and Zhang, L. (2015) Enhancement Removal of Crystal Violet Dye Using Magnetic Calcium Ferrite Nanoparticle: Study in Single- and Binary-Solute Systems. *Chemical Engineering Research and Design*, **94**, 726-735. https://doi.org/10.1016/j.cherd.2014.10.013

[7] Wang, Y., Xie, Y., Zhang, Y., Tang, S., Guo, C., Wu, J., *et al.* (2016) Anionic and Cationic Dyes Adsorption on Porous Poly-Melamine-Formaldehyde Polymer. *Chemical Engineering Research and Design*, **114**, 258-267. https://doi.org/10.1016/j.cherd.2016.08.027

[8] Ayad, M.M., El-Nasr, A.A. and Stejskal, J. (2012) Kinetics and Isotherm Studies of Methylene Blue Adsorption onto Polyaniline Nanotubes Base/Silica Composite. *Journal of Industrial and Engineering Chemistry*, **18**, 1964-1969. https://doi.org/10.1016/j.jiec.2012.05.012

[9] Vinu, R. and Madras, G. (2009) Kinetics of Sonophotocatalytic Degradation of Anionic Dyes with Nano-TiO_2. *Environmental Science & Technology*, **43**, 473-479. https://doi.org/10.1021/es8025648

[10] Salima, A., Benaouda, B., Noureddine, B. and Duclaux, L. (2013) Application of *Ulva lactuca* and *Systoceira stricta* Algae-Based Activated Carbons to Hazardous Cationic Dyes Removal from Industrial Effluents. *Water Research*, **47**, 3375-3388. https://doi.org/10.1016/j.watres.2013.03.038

[11] Wang, H. and Ren, Z.J. (2014) Bioelectrochemical Metal Recovery from Wastewater: A Review. *Water Research*, **66**, 219-232. https://doi.org/10.1016/j.watres.2014.08.013

[12] Bailey, S.E., Olin, T.J., Bricka, R.M. and Adrian, D.D. (1999) A Review of Potentially Low-Cost Sorbents for Heavy Metals. *Water Research*, **33**, 2469-2479. https://doi.org/10.1016/S0043-1354(98)00475-8

[13] Eren, E., Afsin, B. and Onal, Y. (2009) Removal of Lead Ions by Acid Activated and Manganese Oxide-Coated Bentonite. *Journal of Hazardous Materials*, **161**, 677-685. https://doi.org/10.1016/j.jhazmat.2008.04.020

[14] Müller, A., Peters, F., Pope, M.T. and Gatteschi, D. (1998) Polyoxometalates: Very Large Clusters-Nanoscale Magnets. *Chemical Reviews*, **98**, 239-272. https://doi.org/10.1021/cr9603946

[15] Pope, M. (1983) Heteropoly and Isopoly Oxometalates. Springer-Verlag, Berlin. https://doi.org/10.1007/978-3-662-12004-0_1

[16] Salavati, H., Tangestaninejad, S., Moghadam, M., Mirkhani, V. and Mohammadpoor-Baltork, I. (2010) Sonocatalytic Oxidation of Olefins Catalyzed by Heteropolyanion-Montmorillonite Nanocomposite. *Ultrasonics Sonochemistry*, **17**, 145-152. https://doi.org/10.1016/j.ultsonch.2009.05.009

[17] Mizuno, N. and Misono, M. (1998) Heterogeneous Catalysis. *Chemical Reviews*, **98**, 199-218. https://doi.org/10.1021/cr960401q

[18] Herrmann, S. (2015) New Synthetic Routes to Polyoxometalate Containing Ionic Liquids: An Investigation of Their Properties. Springer, Berlin. https://doi.org/10.1007/978-3-658-08796-8

[19] Liu, Y., Zheng, R., Han, Z., Gong, K., He, X. and Zhai, X. (2015) Supramolecular Hybrids of Polytungstates and Their Adsorption Properties for Methylene Blue. *Journal of Solid State Chemistry*, **231**, 169-174. https://doi.org/10.1016/j.jssc.2015.08.026

[20] Prabhu, P.P. and Prabhu, B. (2018) A Review on Removal of Heavy Metal Ions from Waste Water Using Natural/Modified Bentonite. *MATEC Web of Conferences*, Vol. 144, Article No. 02021. https://doi.org/10.1051/matecconf/201814402021

[21] Akpomie, K.G., Dawodu, F.A. and Adebowale, K.O. (2015) Mechanism on the Sorption of Heavy Metals from Binary-Solution by a Low Cost Montmorillonite and Its Desorption Potential. *Alexandria Engineering Journal*, **54**, 757-767. https://doi.org/10.1016/j.aej.2015.03.025

[22] Şahin, Ö., Kaya, M. and Saka, C. (2015) Plasma-Surface Modification on Bentonite Clay to Improve the Performance of Adsorption of Methylene Blue. *Applied Clay Science*, **116**, 46-53. https://doi.org/10.1016/j.clay.2015.08.015

[23] Oliveira, C.I.R.d., Rocha, M.C.G., Silva, A.L.N.d. and Bertolino, L.C. (2016) Characterization of Bentonite Clays from Cubati, Paraíba (Northeast of Brazil). *Cerâmica*, **62**, 272-277. https://doi.org/10.1590/0366-69132016623631970

[24] Eren, E. and Afsin, B. (2008) An Investigation of Cu(II) Adsorption by Raw and Acid-Activated Bentonite: A Combined Potentiometric, Thermodynamic, XRD, IR, DTA Study. *Journal of Hazardous Materials*, **151**, 682-691. https://doi.org/10.1016/j.jhazmat.2007.06.040

[25] Tian, N., Zhu, M., Wu, Q., Yan, W. and Yaroslavtsev, A.B. (2014) Preparation and Conductivity of the Keggin-Type Trivanadium-Substituted Tungstosilicic Acid $H_7SiW_9V_3O_{40}\cdot 9H_2O$. *Materials Letters*, **115**, 165-167. https://doi.org/10.1016/j.matlet.2013.10.052

[26] Wu, Q., Sang, X., Liu, B. and Ponomareva, V. (2005) Synthesis and Performance of High-Proton Conductor Undecatungstochromoindic Heteropoly Acid. *Materials Letters*, **59**, 123-126. https://doi.org/10.1016/j.matlet.2004.07.050

[27] De Castro, M.L.F.A., Abad, M.L.B., Sumalinog, D.A.G., Abarca, R.R.M., Paoprasert, P. and de Luna, M.D.G. (2018) Adsorption of Methylene Blue Dye and Cu(II) Ions on EDTA-Modified Bentonite: Isotherm, Kinetic and Thermodynamic Studies. *Sustainable Environment Research*, **28**, 197-205. https://doi.org/10.1016/j.serj.2018.04.001

[28] McKay, G., Ho, Y. and Ng, J. (1999) Biosorption of Copper from Waste Waters: A Review. *Separation and Purification Methods*, **28**, 87-125. https://doi.org/10.1080/03602549909351645

[29] Allen, S.J., Gan, Q., Matthews, R. and Johnson, P.A. (2005) Kinetic Modeling of the Adsorption of Basic Dyes by Kudzu. *Journal of Colloid and Interface Science*, **286**, 101-109. https://doi.org/10.1016/j.jcis.2004.12.043